Supporting Information

Joint Enhancement in the Electrochemical Reversibility and Cycle Lives for Copper Sulfide for Sodium and Potassium-Ion Storage via Selenium Substitution

Hezhe Lin,† Jingyi Liu,† Malin Li,† Nan Chen,† Wei Xuan,*‡ Lina Liu,§ Shiyu Yao,*† FeiDu*†

†Key Laboratory of Physics and Technology for Advanced Batteries (Ministry of Education), State Key Laboratory of Superhard Materials, College of Physics, Jilin University, Changchun 130012, China

‡Department of Hepatopancreaticobiliary Surgery, China-Japan Union Hospital of Jilin University, Changchun 130033, China

§Materials Science and Engineering, Changchun University of Science and Technology, Changchun, Jilin 130022, China

*Email: xuanwei@jlu.edu.cn

*Email: yaoshiyu@jlu.edu.cn

*Email: dufei@jlu.edu.cn

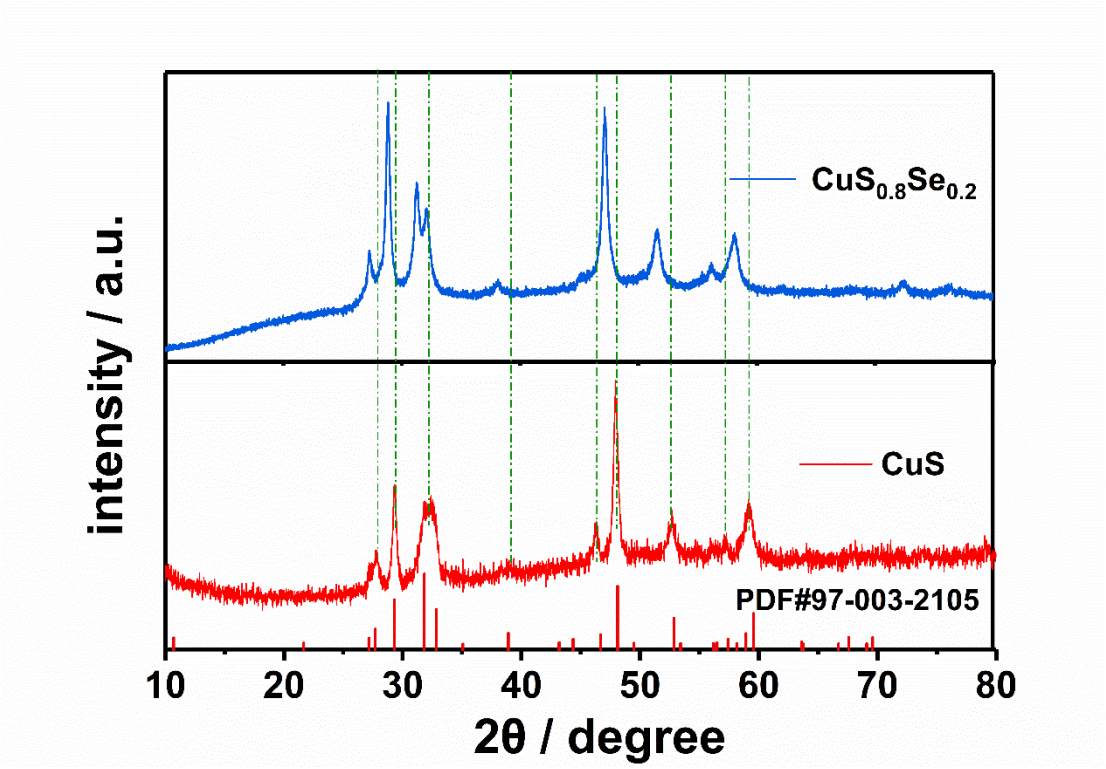

Figure. S1 XRD pattern of $CuS_{0.8}Se_{0.2}$ and CuS with the standard XRD pattern of CuS for identification.

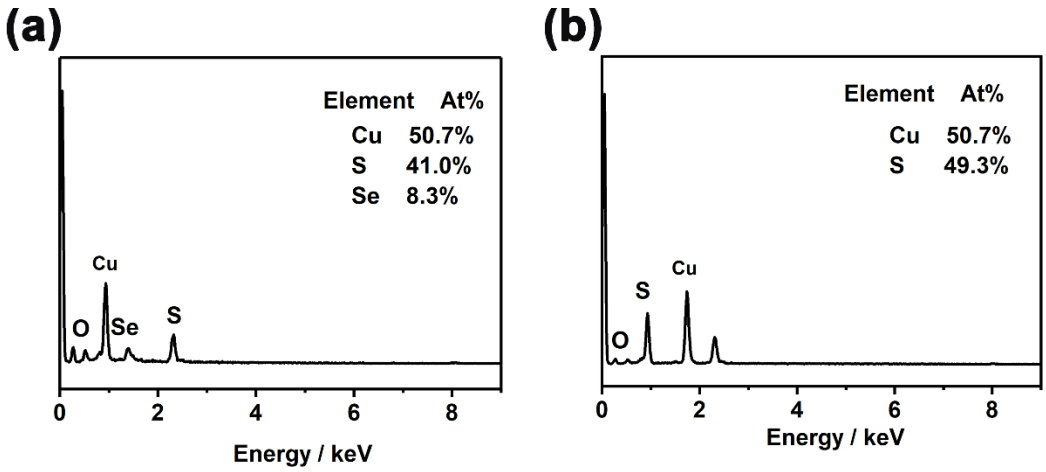

Figure. S2 EDX patterns of $CuS_{0.8}Se_{0.2}$ **a)** and CuS **b).**

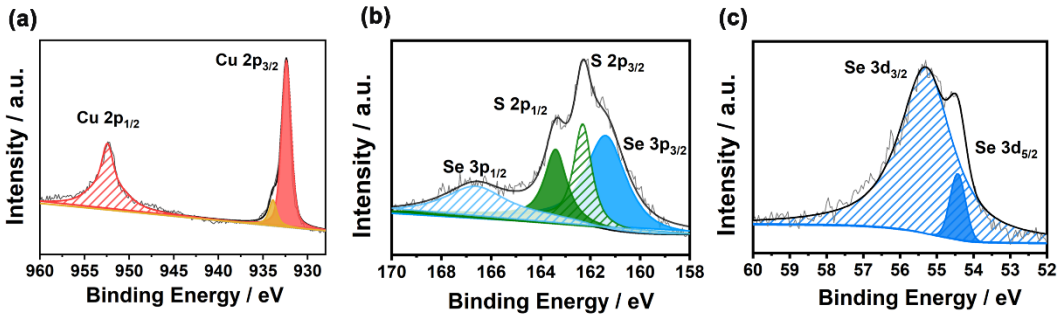

Figure. S3 The high-resolution XPS spectra of **a)** Cu 2p, **b)** S 2p and Se 3p, and **c)** Se 3d for the $CuS_{0.8}Se_{0.2}$ sample.

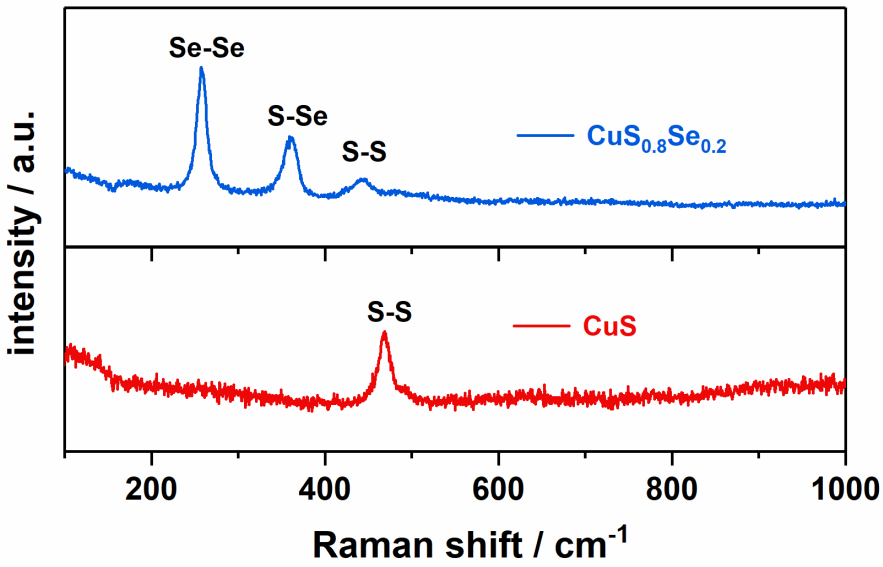

Figure. S4 Raman spectrum of nanosheets $CuS_{0.8}Se_{0.2}$ and CuS.

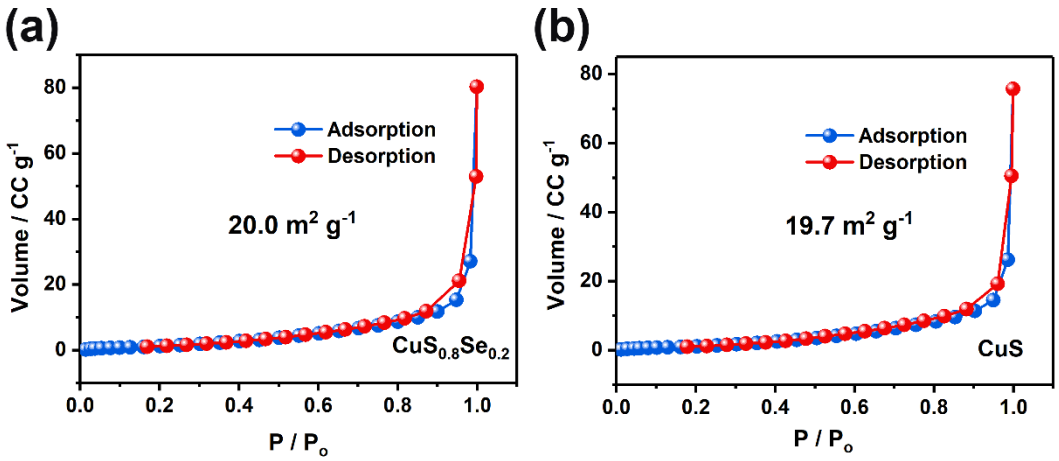

Figure. S5 Nitrogen adsorption-desorption isotherms of **a)** $CuS_{0.8}Se_{0.2}$, **b)** CuS.

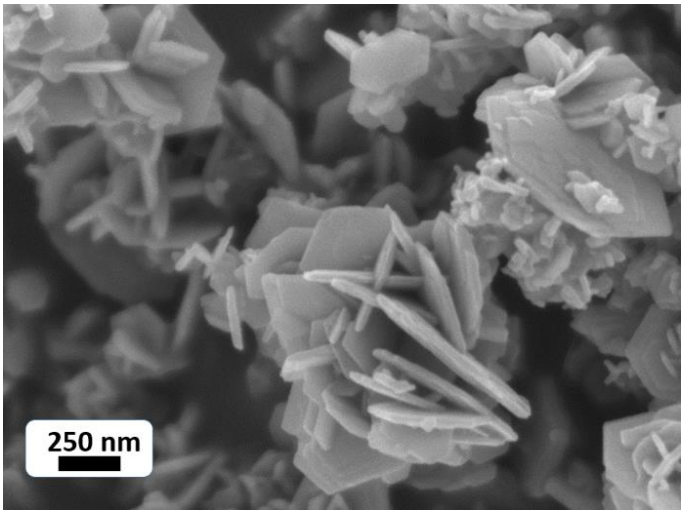

Figure. S6 SEM images of CuS.

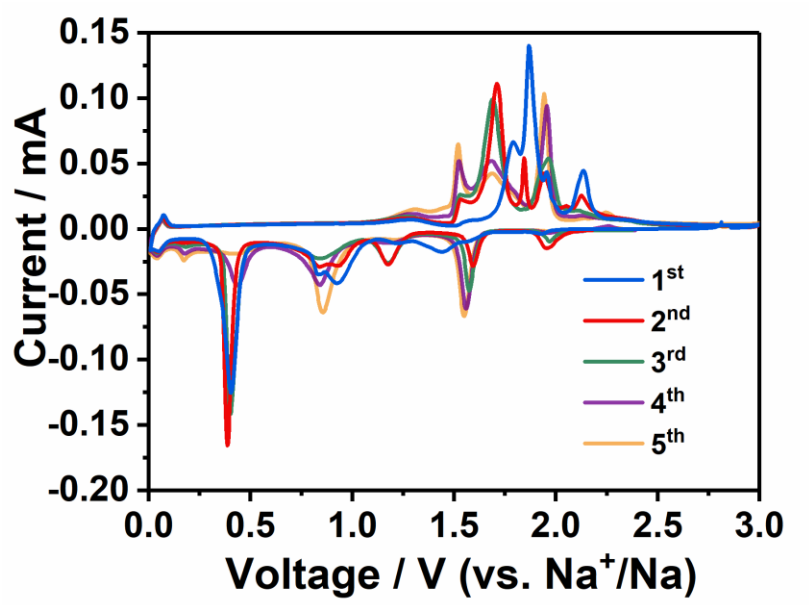

Figure. S7 CV curves of CuS electrode at a scan rate of 0.1 mV s^{-1}**.**

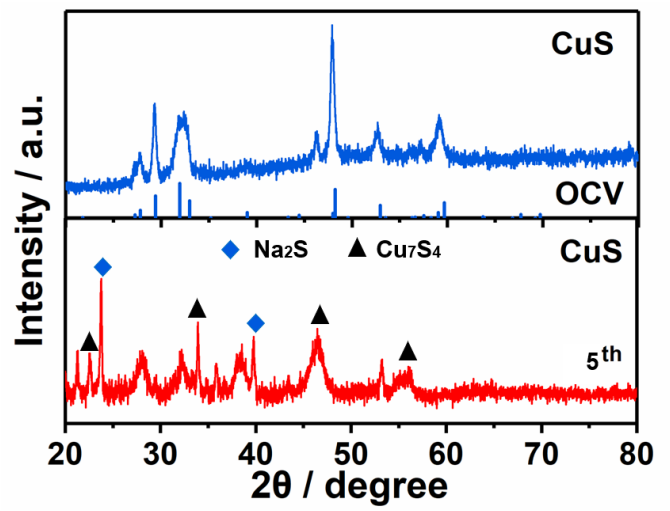

Figure. S8 XRD pattern of CuS at OCV and the 5th cycle.

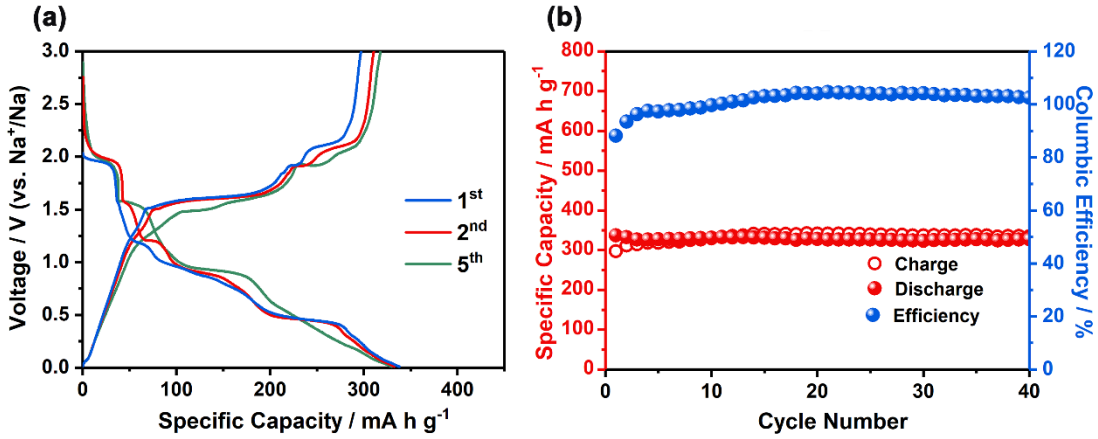

Figure. S9 **a)** Galvanostatic charge-discharge curves and **b)** cycle performance of CuS.

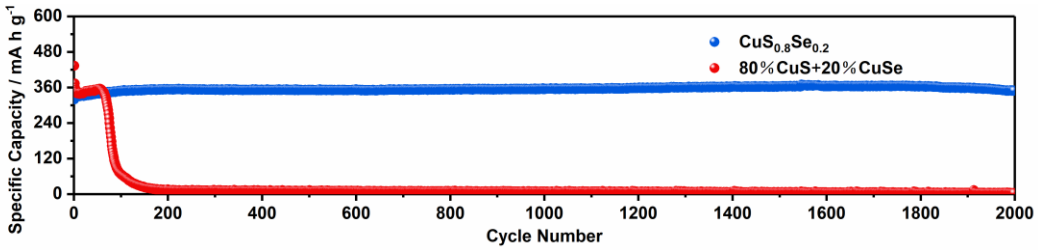

Figure. S10 Cycling performance of $CuS_{0.8}Se_{0.2}$ and mixture of the hexagonal CuS and CuSe in a ratio of 4:1.

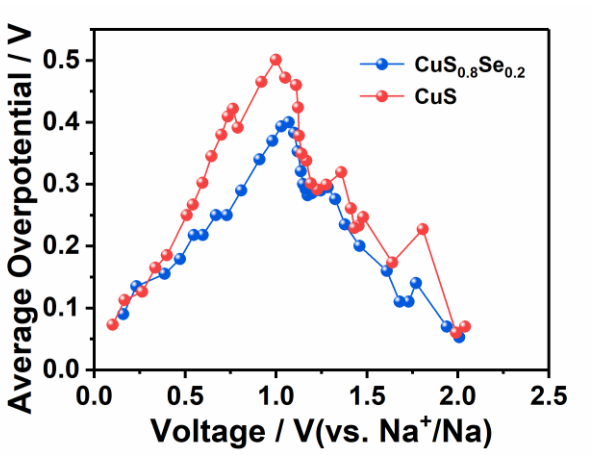

Figure. S11 Comparison of capacity and cycle performance of $CuS_{0.8}Se_{0.2}$ and CuS.

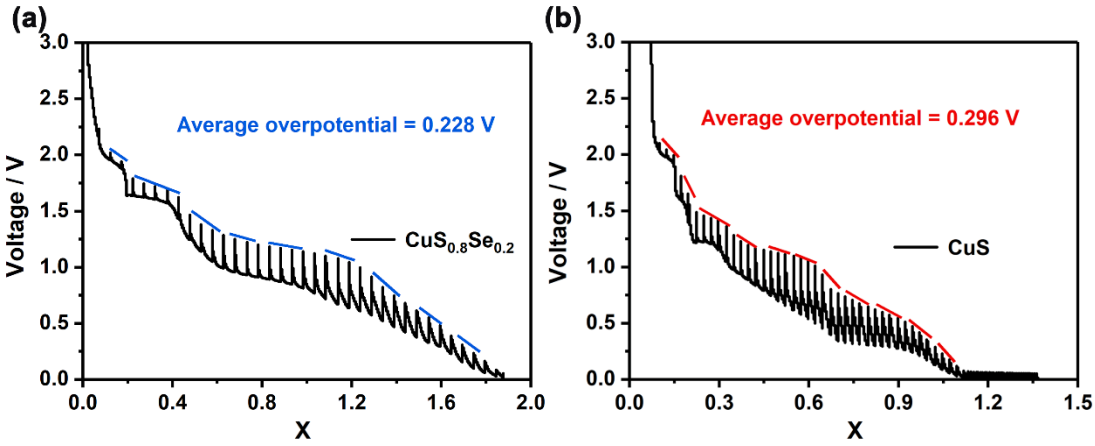

Figure. S12 GITT curves of **a)** $CuS_{0.8}Se_{0.2}$ and **b)** CuS.

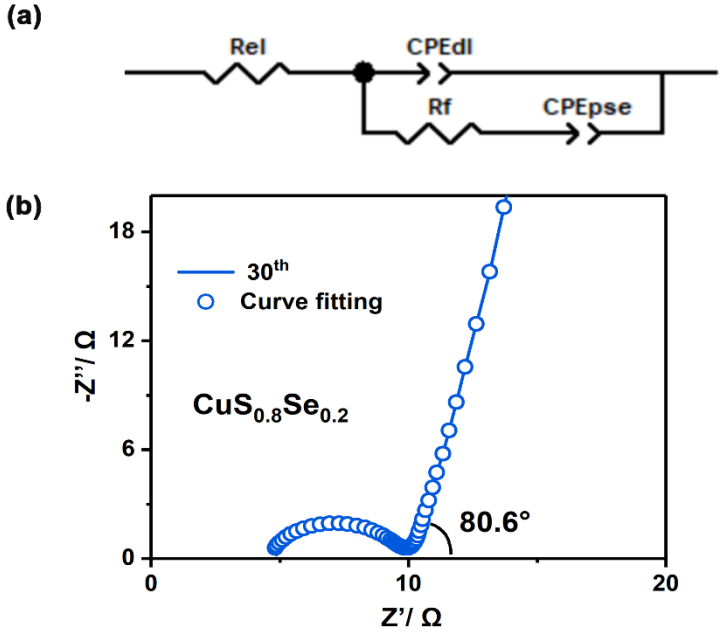

Figure. S13 Nyquist representations of impedance data of CuSe for SIBs, circuit model describing the impedance behavior of CuSe electrodes is shown in the inset.

The angle between straight line and Z'-axis is 80.6° , which is closer to behavior of constant phase element (Z_{CPE}) rather than Warburg element. Thus Figure S13a shows the circuit model to describe the electrochemical impedance behavior. R el and R_f corresponds to resistance of electrolyte and charge transfer resistance. CPE dl is corresponding to double-layer capacitance near electrode and CPE pse is related to pseudocapacitance. $Z_{CPE\ dl}$ is given by equation:

$$Z_{CPE} = 1/B(j\omega)^{n}$$

where B and n (0< n< 1) is frequency-independent proportionality constants. [14] The value of n is 1 for ideal capacitor and 0.5 for ideal battery materials. After fitting the curve, value of n is calculated to be 0.90, which suggested a dominant pseudocapacitance.

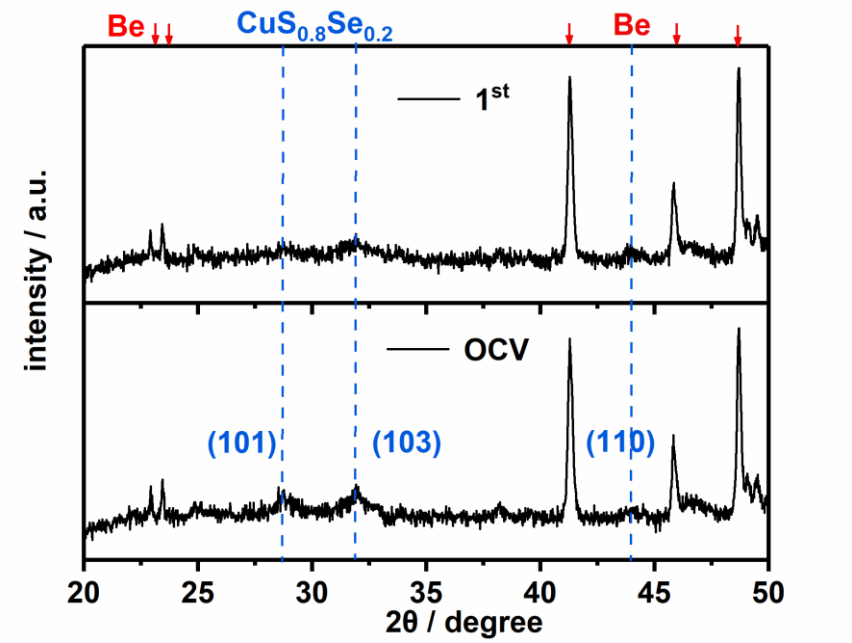

Figure. S14 *In-situ X-ray* diffraction patterns of $CuS_{0.8}Se_{0.2}$ of OCV and after the first cycle.

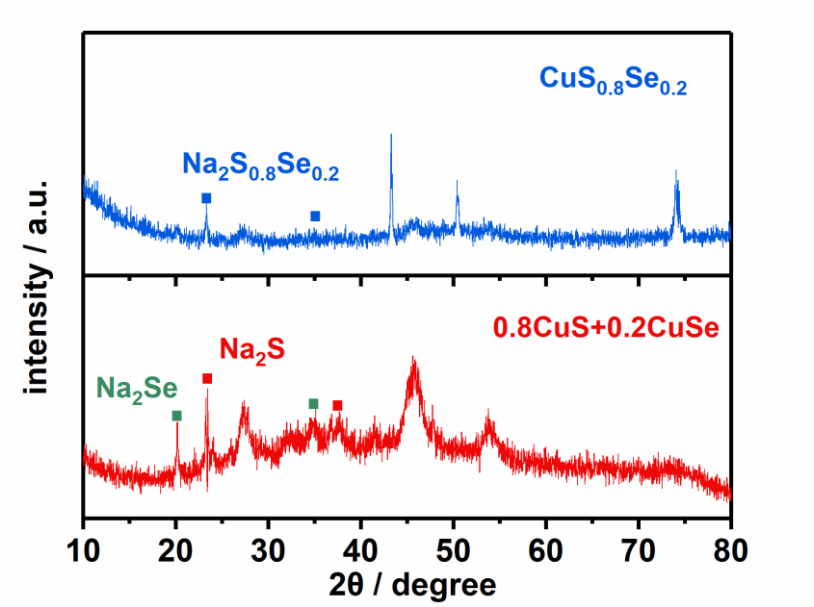

Figure. S15 *Ex-situ X-ray* diffraction patterns of $CuS_{0.8}Se_{0.2}$ and CuS electrode collected after discharging to 0.01V for the first cycle.

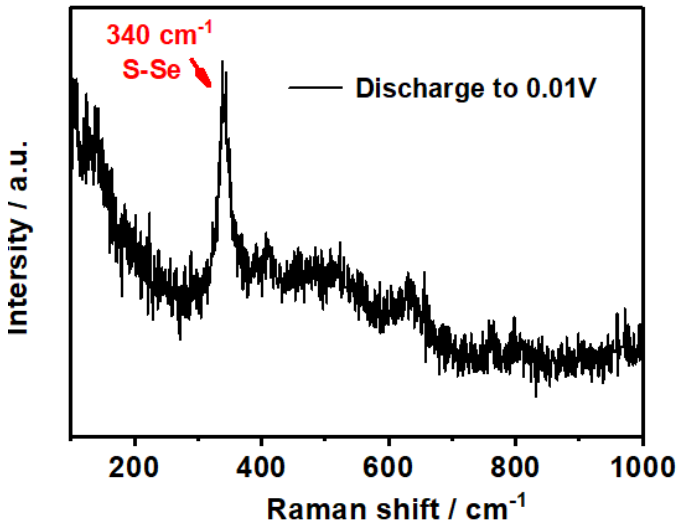

Figure. S16 *Ex-situ* Raman spectrum of nanosheets $CuS_{0.8}Se_{0.2}$ after discharging to 0.01V for the first cycle.

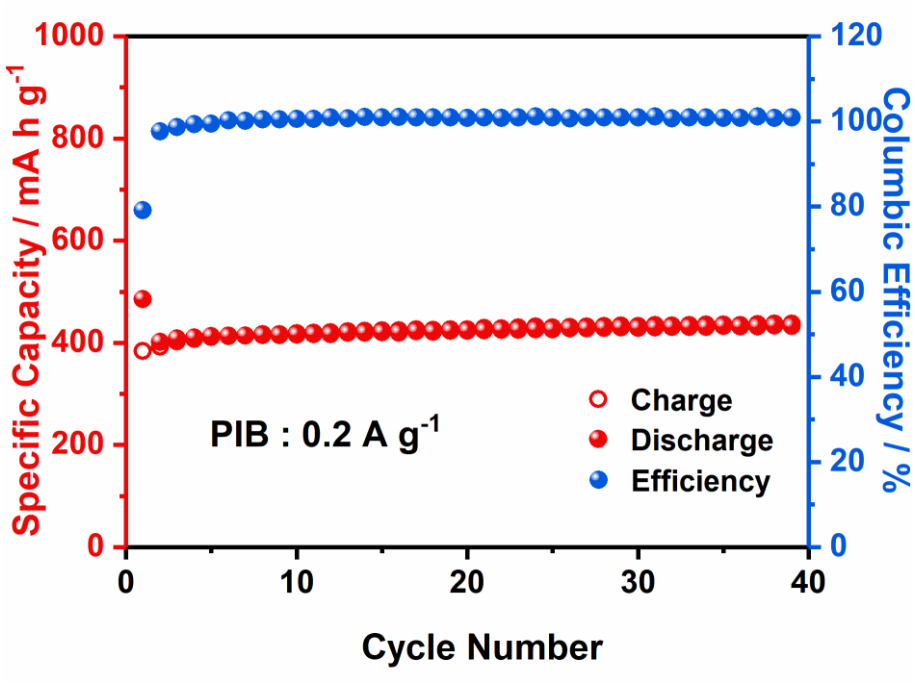

Figure. S17 Cycling performance of $CuS_{0.8}Se_{0.2}$**.**

Table S1.

Rietveld refinement results of $CuS_{0.8}Se_{0.2}$

R_p=1.36 R_{wp}=1.90 R_{exp}=1.93

P63-mmc a=b=3.8504(4) Å, c=16.7227(2) Å, α=β=90°,γ=120°					
Atom	**Wyckoff**	**x**	**y**	**z**	**Occ**
Cu1	**2d**	**0.3333**	**0.6667**	**0.7500**	**1.0**
Cu2	**4f**	**0.3333**	**0.6667**	**0.1005**	**1.0**
Se1	**2c**	**0.3333**	**0.6667**	**0.2500**	**0.2**
Se2	**4e**	**0**	**0**	**0.0632**	**0.2**
S1	**2c**	**0.3333**	**0.6667**	**0.2500**	**0.8**
S2	**4e**	**0**	**0**	**0.0632**	**0.8**

Table S2. Electrochemical performances of CuS materials previously reported for sodium ion batteries.

Material	Capacity	Capacity retention	Initial Coulomb efficiency	Reference
$CuS_{0.8}Se_{0.2}$	**423 mA h g^{-1}**	**96.1% after 2000 cycles at 5A g^{-1}**	**92.3%**	**This work**
CuS	325 mA h g^{-1}	90.6% after 1100 cycles at 10 A g^{-1}	91.6%	[1]
CuS	335 mA h g^{-1}	94.2% after 400 cycles at 1 A g^{-1}	94.3%	[2]
CuS@CoS_2	304 mA h g^{-1}	79% after 500 cycles at 5 A g^{-1}	88.2%	[3]
GO/CuS	248 mA h g^{-1}	81.3% after 100 cycles at 0.1C	75.5%	[4]
CuS-NDs	366 mA h g^{-1}	80.1% after 500 cycles at 2 A g^{-1}	88.9%	[5]
CuS-CNT	590 mA h g^{-1}	95% after 100 cycles at 2 mA cm^{-2}	94%	[6]
PNL-CuS	420 mA h g^{-1}	92.1% after 1000 cycles at 5 A g^{-1}	95%	[7]
CuS	87mA h g-^{1}	34.6% after 100 cycles at 0.31 A g^{-1}	91%	[8]
Cu_9S_5@NC	230 mA h g^{-1}	79% after 4000 cycles at 2 A g^{-1}	90.6%	[9]
ZnS/CuS@C	282 mA h g^{-1}	91.2% after 2000 cycles at 2 A g^{-1}	86.6%	[10]
Cu_3PS_4	400 mA h g^{-1}	73.4% after 1400 cycles at 1 A g^{-1}	81.8%	[11]
Cu_2S	343 mA h g^{-1}	97.1% after 1400 cycles at 1 A g^{-1}	75.3%	[12]
CuS	418 mA h g^{-1}	87.3% after 100 cycles at 0.1 A g^{-1}	91.6%	[13]

Cu7S4 /CNF	225 mA h g^{-1}	44.1% after 725 cycles at 2 A g^{-1}	88.3%	[14]
CuS	349 mA h g^{-1}	95.8% after 1200 cycles at 5 A g^{-}	89.3%	[15]
CuS@N-C	300 mA h g^{-1}	94.3% after 1200 cycles at 5 A g	82%	[16]
Cu_2S@C@MoS_2	359 mA h g^{-1}	91.7% after 400 cycles at 1 A g	66.7%	[17]
CuS-RGO-2	345 mA h g^{-1}	93.6% after 450 cycles at 1 A g	94.7%	[18]
CuS-150	213 mA h g^{-1}	85.6% after 2000 cycles at 1 5A g	94.1%	[19]

Table S3. Charge transfer resistance of $CuS_{0.8}Se_{0.2}$ and CuS for OCV, 1st and 30th cycle.

Rct	OCV	1st	30th
$CuS_{0.8}Se_{0.2}$	**2.6(3) Ω**	**3.0(1) Ω**	**6.4(4) Ω**
CuS	**3.7(2) Ω**	**3.1(7) Ω**	**58.9(3) Ω**

Table S4. Electrochemical performances of previously reported transition metal sulfide in PIBs

Material	Capacity retention	Initial Coulomb efficiency	Reference
$CuS_{0.8}Se_{0.2}$	**412 mA h g^{-1} at 0.1 A g^{-1}**	**79.1%**	**This work**
	374mA h g^{-1} at 5 A g^{-1}		
VS2	360 mA h g^{-1} at 0.1 A g^{-1}	59.2%	[20]
	280 mA h g^{-1} at 5 A g^{-1}		
CoS	499 mA h g^{-1} at 0.2 A g^{-1}	66.1%	[21]
	276 mA h g^{-1} at 5 A g^{-1}		
FeS	412 mA h g^{-1} at 0.1 A g^{-1}	74.2%	[22]
	139 mA h g^{-1} at 2 A g^{-1}		
MoS2/C	510 mA h g^{-1} at 0.1 A g^{-1}	75.5%	[23]
	260 mA h g^{-1} at 5 A g^{-1}		
Cu_2S	354 mA h g^{-1} at 0.1 A g^{-1}	88.9%	[24]
	297 mA h g^{-1} at 5 A g^{-1}		

REFERENCES

[1] Xiao, Y.; Su, D.; Wang, X.; Wu, S.; Zhou, L.; Shi, Y.; Fang, S.; Cheng, H.-M.; Li, F., CuS Microspheres with Tunable Interlayer Space and Micropore as a High-Rate and Long-Life Anode for Sodium-Ion Batteries. Advanced Energy Materials 2018, 8 (22).

[2]. Yang, Z.; Wu, Z.; Liu, J.; Liu, Y.; Gao, S.; Wang, J.; Xiao, Y.; Zhong, Y.; Zhong, B.; Guo, X., Platelet-like CuS impregnated with twin crystal structures for high performance sodium-ion storage. Journal of Materials Chemistry A 2020, 8 (16), 8049-8057.

[3]. Fang, Y.; Guan, B. Y.; Luan, D.; Lou, X. W. D., Synthesis of CuS@CoS2 Double-Shelled Nanoboxes with Enhanced Sodium Storage Properties. Angew Chem Int Ed Engl 2019, 58 (23), 7739-7743.

[4]. Liu, W.; Shi, B.; Wang, Y.; Li, Y.; Pei, H.; Guo, R.; Hou, X.; Zhu, K.; Xie, J., A Flexible, Binder-Free Graphene Oxide/Copper Sulfides Film for High-Performance Sodium Ion Batteries. ChemistrySelect 2018, 3 (20), 5608-5613.

[5]. Kim, N. R.; Choi, J.; Yoon, H. J.; Lee, M. E.; Son, S. U.; Jin, H.-J.; Yun, Y. S., Conversion Reaction of Copper Sulfide Based Nanohybrids for Sodium-Ion Batteries. ACS Sustainable Chemistry & Engineering 2017, 5 (11), 9802-9808.

[6]. Gross, M. M.; Manthiram, A., Development of low-cost sodium-aqueous polysulfide hybrid batteries. Energy Storage Materials 2019, 19, 346-351.

[7]. Yu, D.; Li, M.; Yu, T.; Wang, C.; Zeng, Y.; Hu, X.; Chen, G.; Yang, G.; Du, F., Nanotube-assembled pine-needle-like CuS as an effective energy booster for sodium-ion storage. Journal of Materials Chemistry A 2019, 7 (17), 10619-10628.

[8]. Shi, B.; Liu, W.; Zhu, K.; Xie, J., Synthesis of flower-like copper sulfides microspheres as electrode materials for sodium secondary batteries. Chemical Physics Letters 2017, 677, 70-74.

[9]. Fang, Y.; Yu, X. Y.; Lou, X. W. D., Bullet-like Cu9S5 Hollow Particles Coated with Nitrogen-Doped Carbon for Sodium-Ion Batteries. Angew Chem Int Ed Engl 2019, 58 (23), 7744-7748.

[10]. Zhao, W.; Gao, L.; Yue, L.; Wang, X.; Liu, Q.; Luo, Y.; Li, T.; Shi, X.; Asiri, A. M.; Sun, X., Constructing a hollow microflower-like ZnS/CuS@C heterojunction as an effective ion-transport booster for an ultrastable and high-rate sodium storage anode. Journal of Materials Chemistry A 2021, 9 (10), 6402-6412.

[11]. Brehm, W.; Santhosha, A. L.; Zhang, Z.; Neumann, C.; Turchanin, A.; Martin, A.; Pinna, N.; Seyring, M.; Rettenmayr, M.; Buchheim, J. R.; Adelhelm, P., Copper Thiophosphate (Cu3PS4) as Electrode for Sodium- Ion Batteries with Ether Electrolyte. Advanced Functional Materials 2020, 30 (19).

[12]. Wang, J.; Okabe, J.; Urita, K.; Moriguchi, I.; Wei, M., Cu2S hollow spheres as an anode for high-rate sodium storage performance. Journal of Electroanalytical Chemistry 2020, 874.

[13]. Wu, L.; Gao, J.; Qin, Z.; Sun, Y.; Tian, R.; Zhang, Q.; Gao, Y., Deactivated-desulfurizer-derived hollow copper sulfide as anode materials for advanced sodium ion batteries. Journal of Power Sources 2020, 479.

[14]. Zhang, L.; Wang, Q.; Qiang, C.; Liu, M.; Wang, Q.; Chen, S.; Guo, J.; Fang, Z., Fixing Cu7S4 nanocrystals on flexible carbon nanotube film for distinguished sodium storage performance. Chemical Engineering Journal 2021, 418.

[15]. Yang, Z. G.; Wu, Z. G.; Hua, W. B.; Xiao, Y.; Wang, G. K.; Liu, Y. X.; Wu, C. J.; Li, Y. C.; Zhong, B. H.; Xiang, W.; Zhong, Y. J.; Guo, X. D., Hydrangea-Like CuS with Irreversible Amorphization Transition for High-Performance Sodium-Ion Storage. Adv Sci (Weinh) 2020, 7 (11), 1903279.

[16]. Liu, X.; Li, X.; Lu, X.; He, X.; Jiang, N.; Huo, Y.; Xu, C.; Lin, D., Metal-organic framework derived in-situ nitrogen-doped carbon-encapsulated CuS nanoparticles as high-rate and long-life anode for sodium ion batteries. Journal of Alloys and Compounds 2021, 854.

[17]. Fang, Y.; Luan, D.; Chen, Y.; Gao, S.; Lou, X. W. D., Rationally Designed Three-Layered Cu2S@Carbon@MoS2 Hierarchical Nanoboxes for Efficient Sodium Storage. Angew Chem Int Ed Engl 2020, 59 (18), 7178-7183.

[18]. Li, J.; Yan, D.; Lu, T.; Qin, W.; Yao, Y.; Pan, L., Significantly Improved Sodium-Ion Storage Performance of CuS Nanosheets Anchored into Reduced Graphene Oxide with Ether-Based Electrolyte. ACS Appl Mater Interfaces 2017, 9 (3), 2309-2316.

[19]. Zhang, L.; Hu, Y.; Liu, Y.; Bai, J.; Ruan, H.; Guo, S., Tunable CuS nanocables with hierarchical nanosheet-assembly for ultrafast and long-cycle life sodium-ion storage. Ceramics International 2021, 47 (10), 14138-14145.

[20]. Zhou, J.; Wang, L.; Yang, M.; Wu, J.; Chen, F.; Huang, W.; Han, N.; Ye, H.; Zhao, F.; Li, Y.; Li, Y., Hierarchical VS2 Nanosheet Assemblies: A Universal Host Material for the Reversible Storage of Alkali Metal Ions. Adv Mater 2017, 29 (35).

[21]. Gao, H.; Zhou, T.; Zheng, Y.; Zhang, Q.; Liu, Y.; Chen, J.; Liu, H.; Guo, Z., CoS Quantum Dot Nanoclusters for High- Energy Potassium- Ion Batteries. Advanced Functional Materials 2017, 27 (43).

[22]. Yu, Q.; Hu, J.; Gao, Y.; Gao, J.; Suo, G.; Zuo, P.; Wang, W.; Yin, G., Iron sulfide/carbon hybrid cluster as an anode for potassium-ion storage. Journal of Alloys and Compounds 2018, 766, 1086-1091.

[23]. Yao, K.; Xu, Z.; Ma, M.; Li, J.; Lu, F.; Huang, J., Densified Metallic MoS2/Graphene Enabling Fast Potassium- Ion Storage with Superior Gravimetric and Volumetric Capacities. Advanced Functional Materials 2020, 30

[24]. Peng, Q.; Zhang, S.; Yang, H.; Sheng, B.; Xu, R.; Wang, Q.; Yu, Y., Boosting Potassium Storage Performance of the Cu2S Anode via Morphology Engineering and Electrolyte Chemistry. ACS Nano 2020, 14 (5), 6024-6033.